Two-time-scale analysis of a ring of coupled vibratory gyroscopes

Huy Vu,[1,*] Antonio Palacios,[1,†] Visarath In,[2,‡] Patrick Longhini,[2,§] and Joseph D. Neff[2,‖]
[1]*Nonlinear Dynamical Systems Group, Department of Mathematics, San Diego State University, San Diego, California 92182, USA*
[2]*Space and Naval Warfare Systems Center, Code 2363, 53560 Hull Street, San Diego, California 92152-5001, USA*
(Received 16 December 2009; published 9 March 2010)

A coupling inertial navigation sensor (INS) system may proven to be beneficial for performance improvement, especially when the manufacturing yield is very low for meeting the specification requirement of various applications. For instance, navigation grade sensors using the current fabrication process would yield one in every few hundreds which would meet the specification requirement after careful selection process and testing. We propose to couple these sensors by putting together the "low grade" sensors in a small array of particular coupling topology to explore their stability properties of known parameter variations produced during the fabrication process. By coupling them in a particular way one may improve the system stability to effect the performance of the INS. Thus in this work we present a coupled inertial navigation sensor (CINS) system consisting of a ring of vibratory gyroscopes coupled through the driving axis of each individual gyroscope. Numerical simulations show that under certain conditions, which depend mainly on the coupling strength, the dynamics of the individual gyroscopes will synchronize with one another. The same simulations also show an optimal network size at which the effects of noise can be minimized, thus yielding a reduction in the phase drift. We quantify the reduction in the phase drift and perform an asymptotic analysis of the motion equations to determine the conditions for the existence of the synchronized state. The analysis yields an analytical expression for a critical coupling strength at which different nonzero mean oscillations merge in a pitchfork bifurcation; passed this critical coupling the synchronized state becomes locally asymptotically stable. The Liapunov-Schmidt (LS) reduction is then applied to determine the stability properties of the synchronized solution and to further show that the pitchfork bifurcation can be subcritical or supercritical, depending on the coefficient of the nonlinear terms in the equations of motion.

DOI: 10.1103/PhysRevE.81.031108 PACS number(s): 05.90.+m, 02.50.Ey, 85.25.Dq, 46.40.−f

I. INTRODUCTION

A generic feature of many nonlinear dynamical systems is high sensitivity, specially near the onset of a bifurcation, to small perturbations. Tiny changes in an operation parameter or material imperfections, for instance, can lead to drastically different responses in the systems output, including nondeterministic behavior. Such sensitivity has been exploited by scientists and engineers to develop novel applications for signal detection and amplification [1–4].

Recently, we have discovered through several theoretical and experimental works [5–9] that coupling a certain number of nonlinear units in some fashion can lead to further enhancements in sensitivity and signal output response relative to background noise. In those works we have introduced model-independent ideas and have demonstrated their applicability to a large class of nonlinear devices whose behavior is governed by overdamped bistable dynamics of the form $\dot{x}=-\nabla U(x)$, where $U(x)$ is a potential energy function. Examples include: fluxgate magnetometers, electric-field sensors, and superconducting quantum interference devices or SQUIDs. In these systems, if the coupling is removed, the individual units are not capable of oscillating on their own. Instead, the state point $x(t)$ will rapidly relax to one of two stable attractors, which correspond to the minima of $U(x)$.

In this work, we investigate further the model-independent ideas of coupling-induced oscillations for enhancement of signal detection, in particular, detection of absolute angles of rotation or rates of angular rotation, through vibratory gyroscopes. Currently, many navigation systems utilize the global positioning system (GPS) to obtain precise position, velocity, and time information. A central problem of the GPS system is its susceptibility to jamming and other interference. The received GPS signal is approximately 20 dB below the ambient noise level or roughly equal to a 50 W light bulb located 11 000 miles away. As a result of this vulnerability and weakness of the system, alternative navigation methods are needed. Many technologies could benefit from the incorporation of a low cost inertial guidance system (IGS) that can operate in situations where the GPS signal is compromised or denied. A prototypical IGS consists of three accelerometers to measure linear movement and three angular rate sensors (gyroscopes) to measure rotational movement. An integrated GPS/IGS unit offers superior performance and jamming robustness but there are no small, low cost angular rate gyroscopes available with acceptable attributes for use in an IGS. Current prototype MEMS (microelectromechanical systems) gyroscopes are compact and inexpensive to produce [10], but their performance characteristics, in particular drift rate, fail to meet the requirements for an inertial grade guidance system. As an alternative approach, we propose a coupled inertial navigation sensor (CINS) system made up of coupled vibratory gyroscopes. The fundamental idea is to synchronize the motion of

*huykhanhvu@yahoo.com
†palacios@euler.sdsu.edu
‡visarath@spawar.navy.mil
§longhini@spawar.navy.mil
‖jdneff@spawar.navy.mil

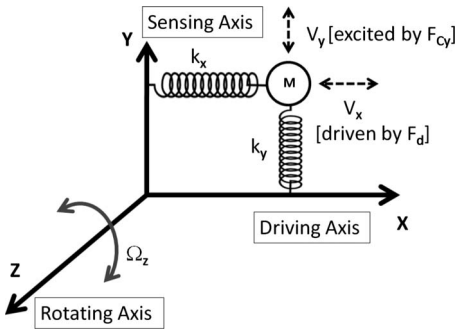

FIG. 1. Schematic of a model for a vibratory gyroscope system. An internal driving force induces the spring-mass system to vibrate in one direction, the x axis in this case. An external rotating force, perpendicular to the plane of the spring-mass system, induces, on the other hand, the spring-mass system to oscillate in the y direction by transferring energy through Coriolis force. The oscillations along the y axis can be used to detect and quantify the rate of rotation.

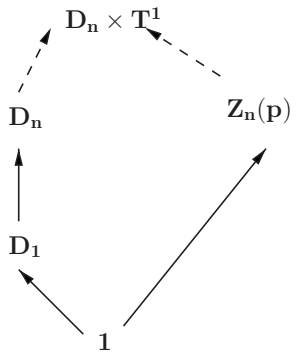

FIG. 2. Lattice of isotropy groups for a CINS ring with $\mathbf{D}_n$-symmetry with arbitrary prime $n>2$.

each gyroscope to the Coriolis driving force, which is proportional to the angular rotation rate, see Fig. 1, so that the collective signal from all gyroscopes can be summed and then demodulated whereas a conventional system requires demodulation electronics for each gyroscope in the array. The summed response from the synchronized array is also larger than the output from a single gyroscope, and thus, it has the potential to enhance its sensitivity while minimizing the negative effects of drift rate. It is worth mentioning that this synchronization state does not occur without a coupling network because of the minor variations in the parameters for each gyroscope and the presence of small nonlinearities in the motion equations. Computer simulations of coupled arrays of gyroscopes have successfully demonstrated that synchronization can be achieved [11–13]. Thus our goal in this work is to determine analytical expressions for the regions of parameter space where such synchronization state occurs, as well as determine its stability properties.

The paper is organized as follows. In Sec. II we introduce the equations of motion that govern the response, i.e., amplitude and phase, of a single vibratory gyroscope. For completeness, an analysis of the frequency response of a single gyroscope via the method of averaging is presented in Appendix A. In Sec. III we formulate the equations of motion for a ring of three gyroscopes coupled bidirectionally along the driving axis. Then we combine ideas and methods from equivariant bifurcation theory with perturbation theory to derive generalized averaged equations in *Normal Form* from abstract, symmetry-based, arguments. An analysis of the normal forms and their fixed point subspaces can then lead us to predict the different classes of behavior of a CINS device with arbitrary number n of gyroscopes before it can be built. We showcase the approach for the particular case of a ring with $n=3$ gyroscopes and perform a stability analysis, via Lyapunov-Schmidt reduction, to determine the stability properties of the synchronized state and the nature of the pitchfork bifurcation by which this state is created. While the phenomenon of coupling-induced synchronization among interconnected oscillators is well known, there is significantly less familiarity in the scientific and engineering communities with the techniques of symmetry breaking as they apply to the engineering, design and fabrication, of complex systems. We believe this work can be a valuable contribution in that direction. We finish the section with a detailed analysis of the effects of noise and variations of the masses. The main results show an optimal network size and an optimal coupling strength at which the effects of material imperfections and signal contamination can be minimized, thus yielding a reduction in the phase drift.

II. VIBRATORY GYROSCOPES

The French mathematician, mechanical engineer, and scientist, Gaspard-Gustave de Coriolis (1792–1843) is best known for the discovery of the "Coriolis" effect: "an apparent deflection and acceleration of moving objects from a straight path when viewed from a rotating frame of reference" [14]. The observed inertial acceleration of the object, also known as Coriolis acceleration, serves nowadays as the basic principle of operation of many inertial navigation systems, including gyroscopes. Vibratory gyroscopes, in particular, are sensor devices that can measure absolute angles of rotation (type I gyroscope) or rates of angular rotation (type II). All vibratory gyroscopes operate on the basis of energy transferred between two vibration modes, a driving mode and a sensing mode, by Coriolis force [15–17]. The conventional model of a vibratory gyroscope consists of a mass-spring system as is shown in Fig. 1. A change in the acceleration around the driving axis caused by the presence of Coriolis force induces a vibration in the sensing axis which can be converted to measure angular rate output or absolute angles of rotation.

The accuracy of most gyroscope systems depend on three parameters: quality factor, phase drift, and robustness. The quality factor is the linear deviation of the measured rate from the true rate (normally given as a percentage of full scale). It characterizes the capability of a gyroscope to accurately sense angular velocity at different angular rates, including the sensitivity of the angular rate sensor and its ability to convert voltage output into angular rate, so its units are in (deg/s)/V. The phase drift is the offset error output that appears as an additive term on the gyroscope output due, mainly, to temperature fluctuations. It characterizes the ability of a gyroscope to reference all rate measurements to the

TABLE I. System parameters for a vibratory gyroscope.

Parameter	Value	Unit
m	1.0E-09	Kg
c_x, c_y	5.1472E-07	N s/m
κ_x, κ_y	2.6494	N/m
μ_x, μ_y	2.933	N/m^3
A_d	1.0E-03	N
w_d	5.165E+04	rad/s

nominal zero rate output, so its units are in deg/s or deg/h. Robustness is the deviation of the measured rate due to noise influence or parameter variations and it is very important because signal processing of the gyroscope output can introduce noise which, in turn, can lead to non-deterministic or stochastic behavior. The units of measurement for the effect of noise are generally deg/$\sqrt{D}$, where D is the intensity of noise.

Equations of motion

The configuration of the vibratory gyroscope of Fig. 1 contains two vibration modes: the *primary* mode (x direction) and the *secondary* mode (y direction). Both modes are coupled to one another by Coriolis force through the term $F_{cx}=|2m\vec{\Omega}_z\times\dot{y}|=2m\Omega_z\dot{y}$ and $F_{cy}=|2m\vec{\Omega}_z\times\dot{x}|=-2m\Omega_z\dot{x}$, respectively, where m is mass and Ω_z is the angular rate of rotation along a perpendicular direction (z axis). The governing equations for the entire spring-mass system can then be written in the following form:

$$m\ddot{x}+c_x\dot{x}+F_r(x)=F_e(t)+2m\Omega_z\dot{y}\quad\text{(drive)},$$

$$m\ddot{y}+c_y\dot{y}+F_r(y)=-2m\Omega_z\dot{x},\quad\text{(sense)},\qquad(1)$$

where c_x (c_y) is the damping coefficient along the x direction (y direction), $F_r(\cdot)$ is the elastic restoring force of the springs. A typical model for the restoring force along the x direction, for instance, has the form: $F_r(x)=\kappa_x x+\mu_x x^3$, where κ_x and μ_x are constant parameters. The same model applies to the y axis, just replace x by y. The x-axis mode, which is also known as the drive axis, is also excited by a reference driving force, typically a periodic signal of the form $F_e=A_d\cos w_d t$, where A_d is the amplitude and w_d is the frequency of the excitation. Typical parameter values, which we will consider in this work, are shown in Table I.

Under these conditions, the gyroscope of Fig. 1 can detect an applied angular rate Ω_z by measuring the displacements along the y axis (also known as sensing axis) caused by the transfer of energy by Coriolis force. If there is no external rotation, i.e., $\Omega_z=0$, the motion equations (1) along the two axes become uncoupled from one another. Furthermore, the dynamics along the x axis reduces to that of a Duffing oscillator subject to a periodic force, which has been extensively studied [18,19]. The motion along the y axis, however, eventually approaches the zero equilibrium due to the absence of any source of energy and also due to the presence of the positive dissipative term c_y. The quality factor parameter for the driving axis is $Q_x=mw_{0x}/c_x$, where $w_{0x}=\sqrt{\kappa_x/m}$ is the natural frequency of oscillation of the mass-spring model in the absence of Coriolis force. Likewise, the quality factor for the sensing axis is $Q_y=mw_{0y}/c_y$, where $w_{0y}=\sqrt{\kappa_y/m}$.

III. BIDIRECTIONALLY COUPLED RING OF GYROSCOPES

We consider an array of N vibratory gyroscopes arranged in a ring configuration, coupled bidirectionally along the drive axis, so that the equations of motion can be written in the general form

$$m_j\ddot{x}_j+c_{xj}\dot{x}_j+F_r(x_j)=F_{ej}(t)+2m_j\Omega_z\dot{y}_j+\sum_{k\to j}c_{jk}h(x_j,x_k),$$

$$m_j\ddot{y}_j+c_{yj}\dot{y}_j+F_r(y_j)=-2m_j\Omega_z\dot{x}_j,$$

where h is the coupling function between gyroscopes j and k, the summation is taken over those gyroscopes k that are coupled to gyroscopes j and c_{jk} is a matrix of coupling strengths. Parameter values are the same as those shown in Table I. We choose to couple the INS system through the drive axis because this type of coupling is the most natural way to add signals on top of the already existing external drive signal. One may also choose to couple through the sense axis but that may involve more design changes and added circuitry to accommodate the input signal. In this section we will consider, in particular, a diffusive coupling function of the form $h(x_j,x_k)=x_k-x_j$. Here we consider the response of the coupled gyroscope system to a weak periodic force, so we apply the transformation $A_d\to\varepsilon$. In an attempt to understand the collective behavior of the network, we make the simplifying assumption of the mass spring dampers to be identical and set all coefficients equal to the mean value for a typical ensemble of gyroscopes. In addition, we assume each gyroscope to be excited by the same external harmonic sine-wave signal with one driving frequency in the drive coordinate axis, i.e., $F_{ei}=F_d\sin w_d t$. Further assuming the coupling strength to be identical, i.e., $c_{jk}=\lambda$, the equations of motion take the form

$$m\ddot{x}_j+c\dot{x}_j+\kappa x_j+\mu x_j^3=\varepsilon\sin w_d t+2m\Omega_z\dot{y}_j+\lambda(x_{j+1}-2x_j+x_{j-1})$$

$$m\ddot{y}_j+c\dot{y}_j+\kappa y_j+\mu y_j^3=-2m\Omega_z\dot{x}_j.\qquad(2)$$

A. Symmetry formalism

A general approach to characterize the amplitude and phase response of a CINS network [Eq. (2)] in response to Coriolis force is to apply again the method of averaging. As we showed in Sec. II, stationary solutions of the averaged equations correspond to periodic solutions of the original nonautonomous model equations (2). But finding those solutions can be, however, a daunting task. In fact, investigation of the much simpler case: uncoupled gyros $\lambda=0$ with no Coriolis force $\Omega_z=0$, which leads to a generic form of the forced Stuart-Landau equation, has a long history, see e.g.,

Appleton [22] in 1922 and Van der Pol [23,24] in 1927. And even in this much simpler case a complete picture was not established until recently by Holmes and Rand [25] and Argyris [26]. In those works the stationary solutions are found by solving a 6-degree polynomial. In the simplest case $n=3$ gyroscopes, a similar approach leads to a nonlinear system of equations of degree 18 in r_x and r_y, which are intractable to direct analysis. Prediction and analysis of other patterns is practically impossible.

Recently, we have been able to gain some initial understanding and insight into the CINS system response by combining equivariant bifurcation theory with perturbation methods. The theory allows us to derive generalized averaged equations in *Normal Form* from abstract, symmetry-based, arguments. An analysis of the normal forms and their fixed point subspaces can then lead us to predict the different classes of behavior of a CINS device before it can be built. Then perturbation methods, and the Lyapunov-Schmidt reduction, can be applied to determine stability boundaries of the solutions of interest, in our case, the synchronized state. Next we present details of this approach.

The gyroscopes are identically coupled to their nearest neighbors in a ring with no preferred orientation, i.e., bidirectionally, then the ring has $\mathbf{D}_n$ symmetry, where $\mathbf{D}_n$ is the Dihedral group of symmetries of an n-gon. Now it is well-known from the averaging theorem [21,27] that the explicit time periodicity contained in the solutions of the original *nonautonomous* equations (2) is expressed as a phase-shift symmetry T^1 of the *autonomous* averaged equations, where T^1 is the circle group: $\{z \in \mathbf{C}:|z|=1\}$. Thus we seek to approximate the asymptotic dynamics of Eq. (2) by the dynamics of a $\Gamma \times T^1$-equivariant vector field on the n-dimensional torus $T^n=T^1 \times \ldots \times T^1$ (n times), where Γ is the group of *global* symmetries induced by the pattern of coupling and T^1 is the phase-shift symmetry of the averaged equations for each individual gyroscope. Let $z=(z_d,z_s,A_d)$ denote the state variable of a gyroscope, where $z_d=r_x(t)e^{iwt+\theta_x(t)}$ and $z_s=r_y(t)e^{iwt+\theta_y(t)}$. Also note that we treat the forcing parameter A_d as a variable. Let T^1 act on $\mathbf{C}^3$ in the standard way; that is, $\theta z=(e^{i\theta}z_d,e^{i\theta}z_s,e^{i\theta}A_d)$. Recall: (a) a real-valued polynomial function $f:\mathbf{C}^3 \to \mathbf{R}$ is invariant under a group Γ if $f(\gamma x)=f(x)$, for all $\gamma \in \Gamma$. (b) A mapping $g:V \to V$ is Γ-equivariant if $g(\gamma x)=\gamma g(x)$, for all $\gamma \in \Gamma$. Direct calculations yield the following result.

(i) A Hilbert basis for the T^1-invariant polynomials on $\mathbf{C}^3$ is

$$u_1 = z_d\bar{z}_d, \quad u_2 = z_s\bar{z}_s, \quad u_3 = A_d\bar{A}_d,$$

$$v_1 = z_d\bar{z}_s,\bar{v}_1, \quad v_2 = z_d\bar{A}_d,\bar{v}_2, \quad v_3 = z_s\bar{A}_d,\bar{v}_3.$$

(ii) The T^1-equivariant maps are generated by

$$\begin{bmatrix} z_d \\ 0 \\ 0 \end{bmatrix}, \quad \begin{bmatrix} z_s \\ 0 \\ 0 \end{bmatrix}, \quad \begin{bmatrix} A_d \\ 0 \\ 0 \end{bmatrix}, \quad \begin{bmatrix} 0 \\ z_d \\ 0 \end{bmatrix}, \quad \begin{bmatrix} 0 \\ z_s \\ 0 \end{bmatrix}, \quad \begin{bmatrix} 0 \\ A_d \\ 0 \end{bmatrix},$$

$$\begin{bmatrix} 0 \\ 0 \\ z_d \end{bmatrix}, \quad \begin{bmatrix} 0 \\ 0 \\ z_s \end{bmatrix}, \quad \begin{bmatrix} 0 \\ 0 \\ A_d \end{bmatrix}.$$

Since A_d is actually a parameter, v_2 and v_3 represent parametrically forced terms which we will not consider in this work. Also, the external force is expected to be held constant so $\dot{A}_d=0$ and the last three equivariant maps are not included. Thus, the normal forms can be written as

$$\frac{dz}{dt} = [g_1(z,A_d),g_2(z,A_d),0],$$

where $g_1=p_1z_d+p_2z_s+p_3A_d$, $g_2=q_1z_d+q_2z_s+q_3A_d$, $p_i's$ and $q_i's$ are complex-valued functions of u_1, u_2, u_3, v_1, v_2, and v_3. Direct derivation (up to third order) yields:

$$\dot{z}_d = \frac{\varepsilon}{2w}\left[\left\{-cw_0w - \left[\Delta - w\gamma - \frac{3\mu}{16w}(|z_d|^2+|z_s|^2)\right]i\right\}z_d + \frac{3\mu}{16w}(z_d\bar{z}_s+z_s\bar{z}_d)z_s - A_di\right],$$

$$\dot{z}_s = \frac{\varepsilon}{2w}\left[\left\{-cw_0w - \left[\Delta - w\gamma - \frac{3\mu}{16w}(|z_d|^2+|z_s|^2)\right]i\right\}z_s + \frac{3\mu}{16w}(z_d\bar{z}_s+z_s\bar{z}_d)z_d - A_di\right],$$

$$\dot{A}_d = 0. \tag{3}$$

We may now write a generalized model for a $\mathbf{D}_n$ symmetric CINS network,

$$\dot{z}_{dj} = g_1(z_{dj},z_{sj},A_d) + h(z_{d,j+1}-z_{dj},z_{dj}-z_{d,j-1}) + h(z_{s,j+1}-z_{sj},z_{sj}-z_{s,j-1}),$$

$$\dot{z}_{sj} = g_2(z_{dj},z_{sj},A_d) + h(z_{d,j+1}-z_{dj},z_{dj}-z_{d,j-1}) + h(z_{s,j+1}-z_{sj},z_{sj}-z_{s,j-1}),$$

$$\dot{A}_d = 0, \tag{4}$$

where $z_j=(z_{dj},z_{sj},A_d)$ denotes the state-variable of gyroscope j. Then the state-variable of a CINS network with n gyroscopes can be expressed as $Z=(z_1,z_2,\ldots,z_n)$. Recall that $\Gamma \times T^1$ is the group of symmetries of the network and that we already discussed *local* symmetries described by the T^1 symmetry of the averaged equations. We now address *global* Γ symmetries induced by the pattern of coupling. It can be shown that a symmetry $\gamma \in \Gamma$ acts on the phase-space Z by

$$\gamma \cdot (z_1, \ldots, z_n) = (z_{\gamma^{-1}(1)}, \ldots, z_{\gamma^{-1}(n)}).$$

Combining local and global symmetries we arrive at the following action for the full system:

$$(\zeta,e^{i\theta})(z_1, \ldots, z_n) = (e^{i\theta}z_{\zeta(1)}, \ldots, e^{i\theta}z_{\zeta(n)}), \tag{5}$$

where $\zeta \in \mathbf{D}_n$. Thus each coordinate z_j is reordered by some element $\zeta \in \mathbf{D}_n$, and, simultaneously, an identical phase

TABLE II. Classification of possible solutions of a $\mathbf{D}_n$-symmetric CINS network obtained through fixed-point subspaces and the lattice of isotropy subgroups, where $n=mk$ runs through all binary factorizations of n.

Isotropy subgroup Σ	Fixed-point subspace solution
$\mathbf{D}_m(k)=\langle\{\sigma^k,k\}\rangle$	In phase
$\mathbf{D}_m(k\sigma)=\langle\{\sigma^k,k\sigma\}\rangle$	In phase
$\mathbf{Z}_m=\langle\{\sigma^k\}\rangle$	In phase
$\mathbf{D}_m(+-)=\langle\{\sigma^{k-1}k,1),(k\sigma,-1)\}\rangle$ for m even	Standing wave
$\mathbf{D}_m(--)=\langle\{\sigma^{k-1}k,1),(k\sigma,-1)\}\rangle$ for k even	Standing wave
$\mathbf{Z}_m(p)=\langle\{\sigma^k,w^{pk}\}\rangle$ where $p\in\{1,\ldots,[m/2]\}$	Traveling wave

translation by an arbitrary angle θ is applied to each z_j. Using the action of $\mathbf{D}_n\times T^1$ we can determine the lattice of isotropy subgroups and find out that there are three classes of solutions as is shown in Table II. Each solution lies in the fixed point subspace of the corresponding isotropy subgroup. Details of the derivation of the lattice can be found in [28].

For example, when $n>2$ is an arbitrary prime number, the lattice *predicts* the existence of two *in-phase* (IP) solution classes, see Fig. 2, one with $\mathbf{D}_n$-symmetry and one with $\mathbf{D}_1$-symmetry, and p *traveling wave* (TW) solutions. In the $\mathbf{D}_n$ solution, all n gyroscopes are expected to be completely synchronized, same phase and amplitude, with identical waveform. In the $\mathbf{D}_1$ solution all n gyroscopes are in-phase but some oscillate with respect to a different mean. In the $\mathbf{Z}_n(p)$ solution, the oscillations are out of phase by $2\pi/n$ forming a traveling wave. The dashed arrows signify that the trivial solution $(0,\ldots,0)$ that has the full $\mathbf{D}_n\times T^1$ symmetry does not exist since each proof mass is oscillating with some phase and amplitude.

Figure 3 shows the corresponding patterns of solutions for the particular case where $n=3$. In this case, $Z=(a,a,a)$ corresponds to the IP solution with $\mathbf{D}_3$ symmetry, while $Z=(a,a,b)$ describes the IP solution with $\mathbf{D}_1$ symmetry, all three gyros are still in phase but one of them oscillates with respect to a different mean. The third solution $Z=(a,e^{2\pi/3}a,e^{4\pi/3}a)$ is the traveling wave pattern with a phase lag of $2\pi/3$. Furthermore, a transition from the IP branch with $\mathbf{D}_1$-symmetry to the IP branch with $\mathbf{D}_3$ symmetry is also predicted by the lattice. When n is even, additional standing wave patterns are possible but the complete-synchronization branch with $\mathbf{D}_n$-symmetry is still present.

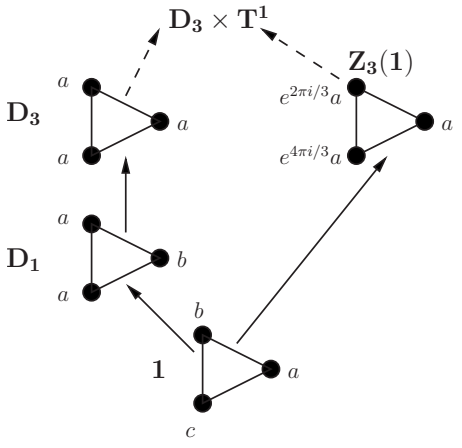

FIG. 3. Patterns of oscillation predicted by the lattice of isotropy subgroups for a CINS ring with $\mathbf{D}_3$ symmetry.

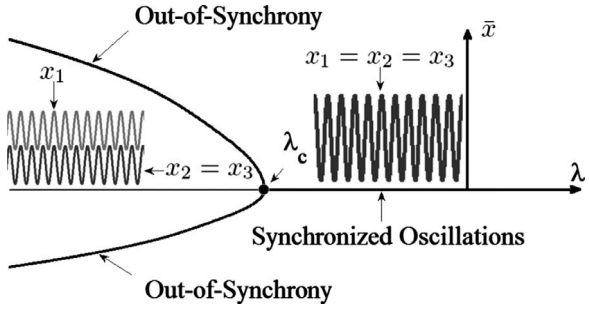

FIG. 4. One-parameter bifurcation diagram illustrating the existence and stability properties of synchronized periodic oscillations in a ring of three vibratory gyroscopes bidirectionally coupled. As λ approaches (from the left) a critical coupling strength, λ_c, three periodic solutions merge in a supercritical pitchfork bifurcation. The stable solutions are periodic solutions with nonzero mean while the unstable solution is the synchronized state in which the driving modes oscillate with the same amplitude and the same phase. Past λ_c the synchronized state becomes locally asymptotically stable, as is supported by numerical calculation of eigenvalues of the linearized vector field.

B. Computational bifurcation analysis

Computer simulations and the continuation software package AUTO [29] confirm the existence of all three solution classes predicted by the lattice of isotropy subgroups for the special case $n=3$, see Fig. 4, including the IP transition $\mathbf{D}_1\rightarrow\mathbf{D}_n$.

The onset of oscillations in the model equations (2) occurs when the coupling strength exceeds a critical value, which we denote by λ_c. When $\lambda<\lambda_c$, there are two stable periodic solutions and one unstable periodic solution. The stable solutions correspond to $Z=(a,a,b)$—two patterns of oscillation in which two of the driving modes oscillate in synchrony but with nonzero mean (one positive and one negative) while the third mode oscillates with a different nonzero mean. The unstable solution represents the complete-synchronization state $Z=(a,a,a)$. As λ increases toward λ_c, the two nonzero mean periodic solution and the zero-mean periodic solution merge in a supercritical pitchfork bifurcation. Past λ_c, only the zero-mean periodic solution exists and becomes locally asymptotically stable (as is determined from the eigenvalues obtained numerically with the aid of AUTO). The oscillations along the sensing axis are, however, unaffected by the change in coupling. They are always stable and completely synchronized with one another though they are out of phase by π with those of the driving axis due to the sign difference in the Coriolis force terms. Next we seek an analytical expression for λ_c as a function of the other system parameters, in particular, as a function of A_d and Ω_z through asymptotic solutions for $x_j(t)$ and $y_j(t)$.

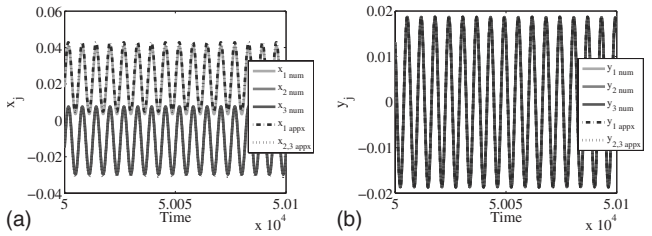

FIG. 5. Time-series solutions of the driving modes, $x_j(t)$, and sensing modes, $y_j(t)$, for a bidirectionally coupled array of three gyroscopes. All solutions are obtained analytically through the asymptotic approximation (6e) and compared against numerical simulations. The accuracy of the approximations is evident and, as expected, when (a) λ is slightly to the left of the critical coupling strength λ_c, both driving and sensing modes oscillate with a nonzero mean. Parameters are: $F_d=0.001$, $\lambda=-0.884$, $\Omega_z=308$.

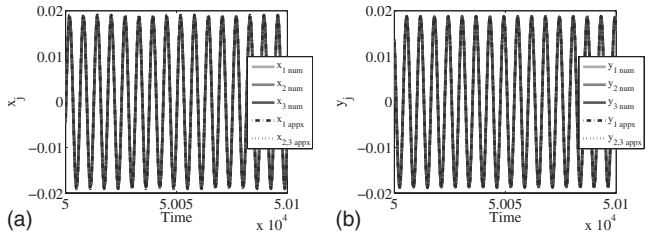

FIG. 6. Comparison of asymptotic approximation and numerical solutions for the driving and sensing modes in a ring of three gyroscopes bidirectionally coupled. Passed the critical coupling strength λ_c, both driving and sensing modes vibrate in complete synchronization among themselves though the oscillations are out of phase by π from one mode to the other. Parameters are: $F_d=0.001$, $\lambda=-0.883$, $\Omega_z=308$.

C. Two-time scale analysis

In order to determine an expansion for $x_j(t)$ and $y_j(t)$ uniformly valid for large times, we introduce two times scales: a fast-time scale $\xi=w_d t$ and a slow-time scale $\eta=\varepsilon t$. In order to introduce these two-time scales into Eq. (2), we need expression for the first and second derivatives of x and y with respect to t, which we obtain by using the chain rule,

$$\frac{dx_j}{dt} = w_d \frac{\partial x_j}{\partial \xi} + \varepsilon \frac{\partial x_j}{\partial \eta}, \tag{6a}$$

$$\frac{d^2x_j}{dt^2} = w_d^2 \frac{\partial^2 x_j}{\partial \xi^2} + 2\varepsilon w_d \frac{\partial^2 x_j}{\partial \xi\, \partial\, \eta} + \varepsilon^2 \frac{\partial^2 x_j}{\partial \eta^2}, \tag{6b}$$

$$\frac{dy_j}{dt} = w_d \frac{\partial y_j}{\partial \xi} + \varepsilon \frac{\partial y_j}{\partial \eta}, \tag{6c}$$

$$\frac{d^2y_j}{dt^2} = w_d^2 \frac{\partial^2 y_j}{\partial \xi^2} + 2\varepsilon w_d \frac{\partial^2 y_j}{\partial \xi\, \partial\, \eta} + \varepsilon^2 \frac{\partial^2 y_j}{\partial \eta^2}. \tag{6d}$$

We also expand x_j and y_j in a truncated Fourier series of ε,

$$x_j = x_{0j} + \varepsilon(x_{1j} + A_{1j}\cos\xi + B_{1j}\sin\xi) + \varepsilon^2(x_{2j} + A_{2j}\cos\xi + B_{2j}\sin\xi + E_{2j}\cos 2\xi + F_{2j}\sin 2\xi) + \cdots, \tag{7a}$$

$$y_j = y_{0j} + \varepsilon(y_{1j} + C_{1j}\cos\xi + D_{1j}\sin\xi) + \varepsilon^2(x_{2j} + C_{2j}\cos\xi + D_{2j}\sin\xi + G_{2j}\cos 2\xi + H_{2j}\sin 2\xi) + \cdots, \tag{7b}$$

Substituting Eqs. (6) and (7) into Eq. (2) yields, after collecting equal powers of ε, a set of partial differential equations (PDE) for each order terms. The technical details of the derivation of these PDES up to $O(\varepsilon^2)$, and their solutions, are shown in Appendix B. We can now use Eq. (7) to reconstruct, up to $O(\varepsilon^2)$, the vibrations along the driving, $x_j(t)$, and sensing, $y_j(t)$, modes. Figures 5 and 6 compare the time series of these reconstructed asymptotic solutions for a ring of three gyroscopes against those from numerical simulations. The accuracy of the approximations is evident.

As expected, when $\lambda<\lambda_c$ both numerical solutions and asymptotic solutions of the driving modes oscillate with nonzero mean. When $\lambda>\lambda_c$, however, the oscillations of the driving modes become entrained with one another, giving rise to a locally asymptotic stable synchronized state. The oscillations between the two modes are out of phase by π due to the difference in signs in the Coriolis-force terms that affect each mode.

D. Onset of synchronization

We estimate the onset of synchronization of the coupled gyroscope system by averaging the values at which the solutions for $x_j(t)$, given by the asymptotic expressions (7), touch zero. Direct calculations yield the critical values in parameters space $(A_{dc},\lambda_c,\Omega_{zc})$, in which we write A_{dc} as a function of λ_c and Ω_{zc}, through

$$A_{dc} = \frac{1}{3}(A_{d_{c1}} + A_{d_{c2}} + A_{d_{c3}}),$$

$$A_{d_{c1}} = \frac{-\|X_{11}\| - \sqrt{\|X_{11}\|^2 - 4(x_{21} - \|X_{21}\|)x_{01}}}{2(x_{21} - \|X_{21}\|)},$$

$$A_{d_{c2}} = \frac{-\|X_{12}\| - \sqrt{\|X_{12}\|^2 - 4(x_{22} - \|X_{22}\|)x_{01}}}{2(x_{21} - \|X_{22}\|)},$$

$$A_{d_{c3}} = A_{d_{c2}},$$

where $\|X_{11}\|=\sqrt{A_{11}^2+B_{11}^2}$, $\|X_{12}\|=\sqrt{A_{12}^2+B_{12}^2}$, $\|X_{21}\|=\sqrt{E_{21}^2+F_{21}^2}$, $\|X_{22}\|=\sqrt{E_{22}^2+F_{22}^2}$. Figure 7 shows a direct comparison of the analytical expression for A_{dc} as a function of coupling strength λ_c, with Ω_z held fixed, against the onset of synchronization obtained through numerical simulations with the aid of the continuation package AUTO [29]. A similar curve is obtained for larger values of Ω_z but with a slight vertical shift that increases as Ω_z increases. In other words, the larger the Coriolis force is the larger the amplitude of the driving force that is required to sustain the synchronization state of the coupled gyroscope system.

Holding now A_d fixed, while varying Ω_z, we obtain the locus of the pitchfork bifurcation λ_c as a function of Ω_z. The locus traces a two-parameter bifurcation diagram shown in Fig. 8.

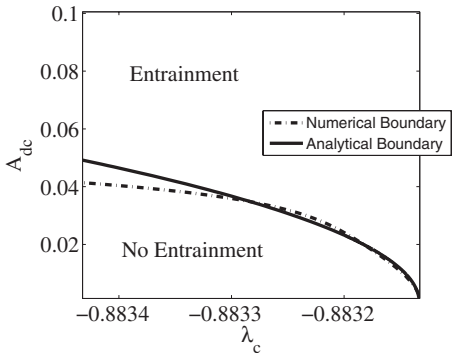

FIG. 7. Two-parameter bifurcation diagram outlines the region of parameter space (A_d,λ) where the vibrations of a system of three gyroscopes, coupled bidirectionally, become completely synchronized. The boundary curve corresponds to the locus of the pitchfork bifurcation where three periodic solutions of the motion equations (2) merge into one as the complete-synchronization state becomes locally asymptotically stable.

It is worth mentioning that the regions of entrainment depicted in Figs. 7 and 8 correspond to local boundaries. In fact, for significantly larger values of A_d, for instance, other types of bifurcations occur including transitions to quasiperiodic motion, see Fig. 9, and even chaotic motion. The analysis of those transitions is beyond the scope of the present work.

E. Robustness

We expect noise in our coupled inertial navigation system to arise from two main sources: fluctuations in the mass of each individual gyroscope and contamination of a target signal. In the former case, we need to replace m in the motion equations by m_i. Informal discussions with experimentalists suggest that a range $m_i=1.0E-09\pm10\%$ is actually reasonable. Variations in other parameters may also occur but for the time being our aim is to get insight into the robustness of the phase drift response of the nonidentical coupled gyroscope system to changes in mass. In the latter case, we consider a target signal contaminated by noise, assumed to be Gaussian band-limited noise having zero mean, correlation time τ_c (usually $\tau_F \ll \tau_c$, where τ_F is the time constant of each individual gyroscope, so that noise does not drive its response), and variance σ^2. This type of noise is a good approximation (except for a small $1/f$ component at very low frequencies) to what is actually expected in an experimental setup. From a modeling point of view, colored noise $\eta(t)$ that contaminates the signal should appear as an additive term in the sensing axis, leading to a stochastic (Langevin) version of the model equations, which for the ring configuration with bidirectional coupling we get

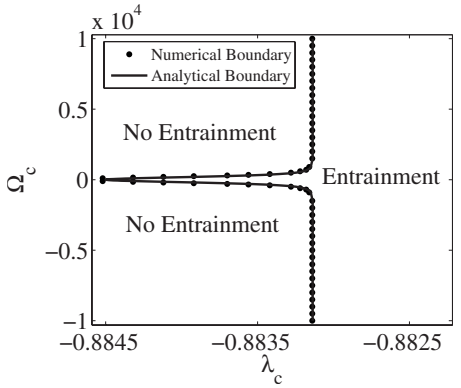

FIG. 8. Two-parameter bifurcation diagram shows the region of parameter space where the vibrations of a system of three gyroscopes, coupled bidirectionally, become completely synchronized. The boundary curve is the same as in Fig. 7 except that A_d is now held fixed at $A_d=0.0001$.

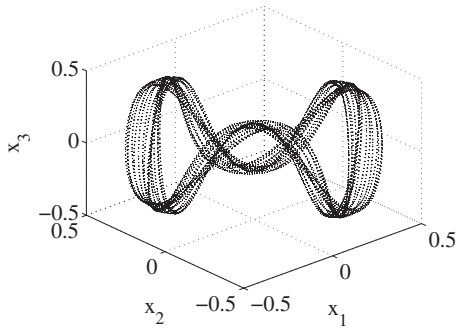

FIG. 9. Torus bifurcation in the driving mode of a coupled system of three gyroscopes, bidirectionally coupled, subject to large amplitude forcing.

$$m_j\ddot{x}_j + c\dot{x}_j + \kappa x_j + \mu x_j^3 = \varepsilon \sin w_d t + 2m_j\Omega_z\dot{y}_j + \lambda(x_{j+1} - 2x_j + x_{j-1}),$$

$$m_j\ddot{y}_j + c\dot{y}_j + \kappa y_j + \mu y_j^3 = -2m_j\Omega_z\dot{x}_j + \eta_j(t),$$

$$\frac{d\eta_j}{dt} = -\frac{\eta_j}{\tau_c} + \frac{\sqrt{2D}}{\tau_c}\xi(t). \tag{8}$$

In general, we would expect somewhat different noise in each equation, since, realistically, the reading of the external signal is slightly different in each sensing axis. This is due to nonidentical circuit elements, mainly. In this work we will consider, therefore, the situation wherein the different noise terms $\eta_i(t)$ are uncorrelated; however, for simplicity, we will assume them to have the same intensity D. Each (colored) noise $\eta_i(t)$ is characterized by $\langle \eta_i(t)\rangle = 0$ and $\langle \eta_i(t)\eta_i(s)\rangle = (D/\tau_c)\times\exp[-|t-s|/\tau_c]$, where $D=\sigma^2\tau_c^2/2$ is the noise intensity, $\xi(t)$ is a Gaussian white noise function of zero mean, and the "white" limit is obtained for vanishing τ_c; in practice, however, the noise is always band limited. In this formulation, we assume the signal to be contaminated purely by external noise; in future work, however, we will also consider other sources of contamination such as internal noise introduced by each individual gyroscope, as well as the coupling and readout circuits.

The new computational bifurcation diagrams (not shown for brevity) are very similar to the one- and two-parameter diagrams shown in Figs. 4, 7, and 8, except that now the critical values of coupling strength λ_c as well as Ω_c and A_{dc} are slighted shifted with respect to those of the identical sys-

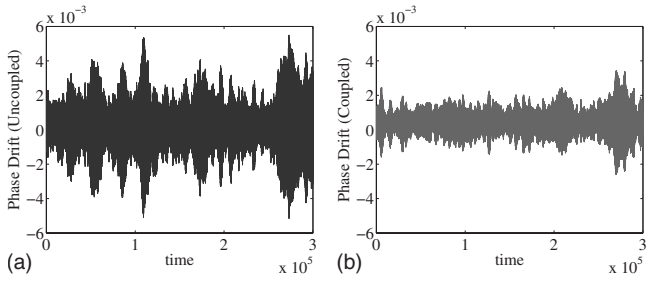

FIG. 10. Comparison of phase drift between (top) an ensemble of three uncoupled gyroscopes and (bottom) a three-gyroscope coupled system. Parameters are: $A_d=0.001$, $\Omega_z=100$, and $\lambda=-0.65$, $m_j=1.0E-09\pm10\%$, and noise intensities $D=\pm1.0E-09$.

tem. Computer simulations of ensembles of various network sizes N of uncoupled and coupled gyroscopes were conducted for comparison purposes of phase drifts. Each ensemble consisted of $M=100$ simulation samples with random fluctuations in mass and noise intensities. The phase of each individual j gyroscope was calculated through $\alpha_j=\arctan(-y_j/w_d y_j)$. Then the phase drift on that individual gyroscope was obtained as the difference between its phase with noise and its phase without noise, i.e., $\theta_j=\alpha_j^{\text{noise}}-\alpha_j^{\text{no noise}}$. Finally, the average phase drift $\theta(t)=(1/MN)\Sigma_{j=1}^{MN}\theta_j$ of the entire ensemble was calculated for both cases, uncoupled and coupled ensembles. Figure 10 shows, in particular, the phase drift of an ensemble of three individual gyroscopes and the phase drift of a similar ensemble but with coupling. The reduction in the phase drift of the sensing axis of the coupled system is, approximately, by a factor of 1.7 times that of the uncoupled system.

To calculate the actual reduction factor we first compute the interquartile range (IQR) of both uncoupled and coupled ensembles. The IQR measures the phase drift variation from the 25% percentile to the 75% percentile. The reduction factor is then the ratio $\text{IQR}(\theta^c)/\text{IQR}(\theta^u)$, where the superscript indicates whether the gyroscopes are coupled or uncoupled, respectively. Figure 11 shows the resulting reduction factors for various network sizes. For small N the reduction factor in

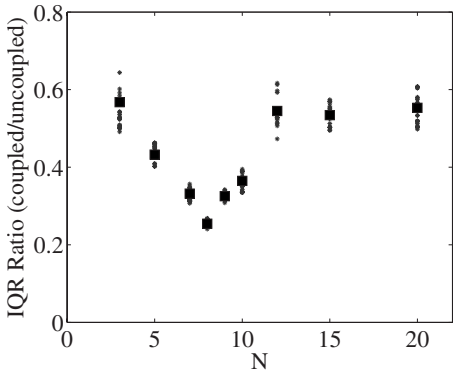

FIG. 11. Reduction factor in the phase drift of a coupled gyroscope system as measured through the interquartile range of ensembles between 80 and 100 samples. Parameters are: $A_d=0.001$, $\Omega_z=100$, $m_j=1.0E-09\pm10\%$ with noise intensities $D=\pm1.0E-09$.

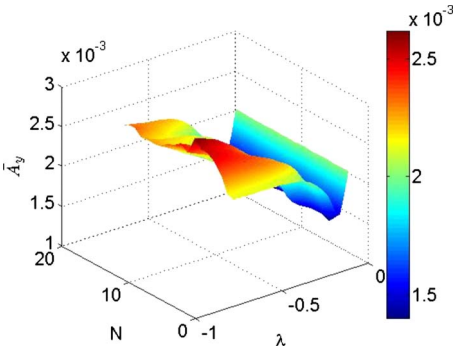

FIG. 12. (Color online) Average amplitude response of the sensing axis of ensembles of coupled gyroscopes with various network sizes and coupling strengths. Parameters are: $A_d=0.001$, $\Omega_z=100$, $m_j=1.0E-09\pm10\%$ without noise.

the phase drift of a coupled vs uncoupled ensemble appears to decrease steadily as N increases but it then increases for networks larger than $N=8$ gyroscopes, approximately. This result suggest an optimal network size where the effects of material imperfections and signal contamination are minimized, thus yielding a reduction in the phase drift.

Careful examination of the average amplitude response of an ensemble of coupled gyroscopes reveals that the amplitude of the sensing axis is dynamically dependent on the number N of gyroscopes and the coupling strength λ, see Fig. 12. In fact, the largest amplitudes are achieved in the vicinity of $N=8$. Larger amplitudes, in turn, can better attenuate the effects of noise and mass fluctuations, and thus, this explains why the bidirectionally coupled gyroscope system yields an optimal phase drift around $N=8$.

IV. DISCUSSION

We have investigated the dynamics of a coupled inertial navigation system consisting of a ring of vibratory gyroscopes coupled through the driving axis of each individual gyroscope. In particular, we considered a ring of $N=3$ (identical) gyroscopes coupled bidirectionally and unidirectionally. In both cases, a numerical bifurcation diagram and a multiple-time scale analysis revealed the existence of an open region in parameter space where the gyroscope become completely synchronized, i.e., they all oscillate with the same wave form and same frequency with identical phases. Computations of the phase differences show that the synchronized state is robust enough to small variations in the mass of the individual gyroscopes, though the phase differences appear to be stronger in the unidirectionally coupled ring. More importantly, numerical simulations reveal an optimal network size, around $N=8$, and coupling strength, approx. $\lambda=-0.65$, where the average amplitude response of the coupled system reaches a maximum. Around this region, the effects of noise on the oscillations of the coupled system are significantly weaker than in the smaller amplitude oscillations of an uncoupled ensemble. This, in turn, allows the coupled system to minimize the effects of noise and material imperfections on its phase drift response.

Experimental design and fabrication of a coupled gyroscope system based on the theoretical findings of this work are being pursuit. The major focus of the experimental work at the moment is to study the behavior of a single gyroscope near bifurcation point due to the change of certain control parameters such as stiffness and excitation force. One idea being pursued for this purpose is to use the coupling mechanism between two gyroscopes to induce a change in the effective linear and nonlinear stiffness parameters. The effective linear and nonlinear stiffness parameters depend on stiffness parameters of the material and the applied voltage. Moreover, the actuation of the coupled devices often depends on the geometry of the structure and the applied voltage. Thus the effects of tuning both linear stiffness and nonlinear stiffness in a system of coupled gyroscopes are currently being investigated by experimental study to observe this dependence.

ACKNOWLEDGMENTS

We gratefully acknowledge support from the Office of Naval Research (Code 30), ONR NREIP and the SPAWAR internal research funding (S&T) program. H.V. and A.P. were supported in part by National Science Foundation Grants No. CMMI-0923803 and No. CMS-0625427. We also would like to acknowledge constructive discussions with Brian K. Meadows at SSC-Pacific, Professor Takashi Hikihara and Suketu Naik at Kyoto University.

APPENDIX A: FREQUENCY RESPONSE OF A SINGLE GYROSCOPE

We now apply the method of averaging [20,21] to solve the equations of motion (1) so that we can characterize the amplitude and phase response of the driving and sensing axes of the gyroscope in response to Coriolis force. Rescaling time as $\tau=w_0 t$, where $w_0=\sqrt{\kappa/m}$ is the natural frequency of oscillation of the unforced system, we can rewrite the equations of motion in the nondimensionalized form,

$$x'' + \varepsilon c w_0 x' + x + \varepsilon \mu x^3 = \varepsilon A_d \cos w\tau + \varepsilon \gamma y',$$

$$y'' + \varepsilon c w_0 y' + y + \varepsilon \mu y^3 = -\varepsilon \gamma x', \tag{A1}$$

where $\varepsilon=1/(mw_0^2)$, $w=(w_d/w_0)$, $\gamma=2mw_0\Omega_z$, and $(\cdot)'$ denotes differentiation with respect to τ.

Using the van der Pol transformation,

$$u_1 = x\cos w\tau - \frac{\dot{x}}{w}\sin w\tau,$$

$$u_2 = -x\sin w\tau - \frac{\dot{x}}{w}\cos w\tau,$$

$$u_3 = y\cos w\tau - \frac{\dot{y}}{w}\sin w\tau,$$

$$u_4 = -y\sin w\tau - \frac{\dot{y}}{w}\cos w\tau,$$

we can rewrite Eq. (1) in a more standard form suitable for the averaging operation, that is

$$\frac{du}{d\tau} = \varepsilon U(u,\tau), \tag{A2}$$

in which $u=(u_1,u_2,u_3,u_4)$ and $U=(U_1,U_2,U_3,U_4)$ is given by

$$\begin{aligned} U_1 = \frac{1}{w}[&-\Delta(u_1\cos w\tau - u_2\sin w\tau) - cw_0 w(u_1\sin w\tau \\ &+ u_2\cos w\tau) + \mu(u_1\cos w\tau - u_2\sin w\tau)^3 \\ &- A_d\cos w\tau + w\gamma(u_3\sin w\tau + u_4\cos w\tau)]\sin w\tau, \end{aligned}$$

$$\begin{aligned} U_2 = \frac{1}{w}[&-\Delta(u_1\cos w\tau - u_2\sin w\tau) - cw_0 w(u_1\sin w\tau \\ &+ u_2\cos w\tau) + \mu(u_1\cos w\tau - u_2\sin w\tau)^3 \\ &- A_d\cos w\tau + w\gamma(u_3\sin w\tau + u_4\cos w\tau)]\cos w\tau, \end{aligned}$$

$$\begin{aligned} U_3 = \frac{1}{w}[&-\Delta(u_3\cos w\tau - u_4\sin w\tau) - cw_0 w(u_3\sin w\tau \\ &+ u_4\cos w\tau) + \mu(u_3\cos w\tau - u_4\sin w\tau)^3 \\ &- w\gamma(u_1\sin w\tau + u_2\cos w\tau)]\sin w\tau, \end{aligned}$$

$$\begin{aligned} U_4 = \frac{1}{w}[&-\Delta(u_3\cos w\tau - u_4\sin w\tau) - cw_0 w(u_3\sin w\tau \\ &+ u_4\cos w\tau) + \mu(u_3\cos w\tau - u_4\sin w\tau)^3 \\ &- w\gamma(u_1\sin w\tau + u_2\cos w\tau)]\cos w\tau, \end{aligned}$$

where $\varepsilon\Delta=w^2-1$. Averaging over the period $T=2\pi/w$ we arrive at the simplified equation:

$$\frac{du}{d\tau} = \varepsilon\bar{U}(u), \tag{A3}$$

where $\bar{U}(u)=\frac{1}{T}\int_0^T U(u,\tau)d\tau$. Explicitly,

$$\begin{aligned} \frac{du}{d\tau} = \frac{\varepsilon}{2w}&\begin{bmatrix} -cw_0 w & \Delta & w\gamma & 0 \\ -\Delta & -cw_0 w & 0 & w\gamma \\ -w\gamma & 0 & -cw_0 w & \Delta \\ 0 & -w\gamma & -\Delta & -cw_0 w \end{bmatrix} u \\ &+ \frac{3\varepsilon\mu}{8w}\begin{bmatrix} -(u_1^2+u_2^2)u_2 \\ (u_1^2+u_2^2)u_1 \\ -(u_3^2+u_4^2)u_4 \\ (u_3^2+u_4^2)u_3 \end{bmatrix} - \frac{\varepsilon}{2w}\begin{bmatrix} 0 \\ A_d \\ 0 \\ 0 \end{bmatrix}. \end{aligned} \tag{A4}$$

In polar coordinates, $r_x=\sqrt{u_1^2+u_2^2}$, $\theta_x=\arctan(u_2/u_1)$, $r_y=\sqrt{u_3^2+u_4^2}$, $\theta_y=\arctan(u_4/u_3)$, we get

$$r_x' = \frac{\varepsilon}{2w}(-cw_0 w r_x - A_d\sin\theta_x + w\gamma r_y\cos\phi),$$

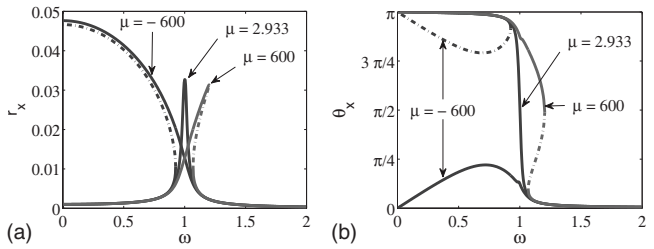

FIG. 13. Frequency response along the driving mode of a nonlinear vibratory gyroscope. Solid lines indicate stable points of Eq. (A5), which are periodic solutions of Eq. (A4), dashed lines represent unstable points.

$$r_x\theta_x' = \frac{\varepsilon}{2w}\left(-\Delta r_x + \frac{3}{4}\mu r_x^3 - A_d\cos\theta_x - w\gamma r_y\sin\phi\right),$$

$$r_y' = \frac{\varepsilon}{2w}(-cw_0 w r_y - w\gamma r_x\cos\phi),$$

$$r_y\theta_y' = \frac{\varepsilon}{2w}\left(-\Delta r_y + \frac{3}{4}\mu r_y^3 - w\gamma r_x\sin\phi\right), \qquad \text{(A5)}$$

where $\phi=\theta_x-\theta_y$. When $\mu\approx 0$ the motion equations of the gyroscope are almost linear and direct calculations show that Eq. (A5) has exactly one stable attractor

$$r_x = \frac{\sqrt{(cw_0w)^2+\Delta^2}}{\Delta_0}, \quad r_y = \frac{wA_d}{\Delta_0}\gamma,$$

where $\Delta_0^2=[(cw_0w)^2+\Delta^2]^2+w^2\gamma^2[2(cw_0w)^2-2\Delta^2+(w\gamma)^2]$. This attractor corresponds to a periodic solution of the original Eqs. (A1) in which both axes oscillate with constant amplitude. The amplitude of the oscillations along the sensing axis, in particular, seem to depend almost linearly on the angular rate of rotation Ω_z. This result is consistent with similar findings by Apostolyuk and Tay [15,16] in their time-average analysis of the dynamics of a linear vibratory gyroscope. The stability of this periodic solution is determined by the eigenvalues of the linear part of Eq. (A4), which direct calculations yield: $\sigma_{1,2}=-cw_0w\pm(\Delta-w\gamma)i$, $\sigma_{3,4}=-cw_0w\pm(\Delta+w\gamma)i$. Since $cw_0w>0$, and considering that there is only one attractor, it follows that both mode of oscillation are locally asymptotically stable. When $|\mu|\gg 0$ the effects of the nonlinear terms in the equations of motion can be significant, thus changing the number of attractors. In fact, computer simulations, see Figs. 13 and 14, indicate that Eq. (A5) has, in general, either one, two, or three attractors. For low w (assuming $w>0$) the simulations show only one stable solution; as w is increased a second stable solution and a saddle-type orbit are created at a saddle-node bifurcation point. At a yet higher frequency the saddle-type orbit annihilates the original stable solution again leaving a single stable solution. A similar transition in the number of equilibrium points occurs for $\mu<0$. This bifurcation scenario leads to a hysteresis behavior in the resonance curves (r_x,w) and (r_y,w) as is illustrated in Figs. 13 and 14.

The multiplicity and stability of the equilibrium points described so far through the resonance curves of Figs. 13 and 14 is reminiscent of those found in the forced Duffing oscillator. This result is expected, after all, the governing equations of the nonlinear gyroscope system and those of the Duffing oscillator are very similar, except for the Coriolis force term. But that term is enough to cause some subtle differences, which are particularly visible at intermediate (negative) values of the nonlinear parameter μ. As is shown in Fig. 15, for $\mu=-200$ a separate pair of branches of equilibrium points appear in both, driving and sensing modes. One branch is stable and one unstable, and each branch corresponds to a periodic solution of the original Eqs. (A4). These periodic solutions limit in a saddle-node point, which merges with the other branches as μ increases (while being negative).

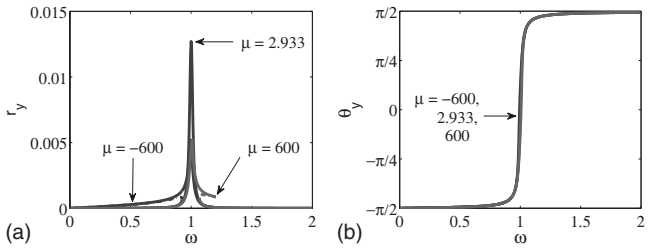

FIG. 14. Frequency response along the sensing mode of a nonlinear vibratory gyroscope along. Solid lines indicate stable points of Eq. (A5), which are periodic solutions of Eq. (A4), dashed lines represent unstable points.

APPENDIX B: TECHNICAL DETAILS OF TWO-TIME SCALE ANALYSIS

Substituting Eqs. (6) and (7) into Eq. (2) and neglecting terms of $O(\varepsilon^3)$, we get, after collecting equal powers of ε, a set of partial differential equations for each order terms. We start with $O(1)$,

$$mw_d^2\frac{\partial^2 x_{0j}}{\partial\xi^2} + cw_d\frac{\partial x_{0j}}{\partial\xi} + \kappa x_{0j} + \mu x_{0j}^3 = 2m\Omega_z w_d\frac{\partial y_{0j}}{\partial\xi} + \lambda(x_{0,j+1} - 2x_{0j} + x_{0,j-1}), \qquad \text{(B1a)}$$

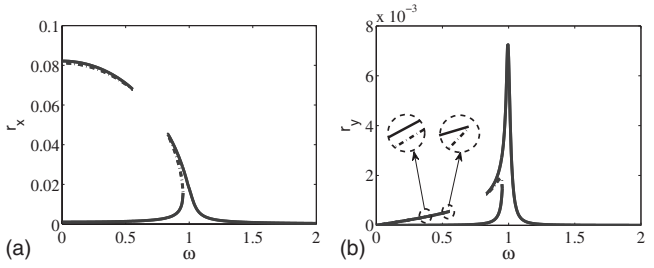

FIG. 15. Frequency response along the driving and sensing mode of a nonlinear vibratory gyroscope, with nonlinear coefficient $\mu=-200$, and rotating rate $\Omega_z=100$. For intermediate (negative) values of μ a separate pair of periodic solutions appear in both, driving and sensing modes. Solid lines indicate stable points, dashed lines represent unstable points.

$$mw_d^2\frac{\partial^2 y_{0j}}{\partial \xi^2}+cw_d\frac{\partial y_{0j}}{\partial \xi}+\kappa y_{0j}+\mu y_{0j}^3=-2m\Omega_z w_d\frac{\partial x_{0j}}{\partial \xi}. \tag{B1b}$$

Since x_{0j} and y_{0j} are equilibrium points (up to $O(1)$) then the derivative terms in Eq. (B1) are all equal to zero, leading to the following set of algebraic equations for x_{0j} and y_{0j},

$$\kappa x_{0j}+\mu x_{0j}^3-\lambda(x_{0,j+1}-2x_{0j}+x_{0,j-1})=0, \tag{B2a}$$

$$\kappa y_{0j}+\mu y_{0j}^3=0. \tag{B2b}$$

Solving for x_{0j} and y_{0j}, we find that Eq. (B2b) admits the following sets of solutions. Set I: $x_{0j}=y_{0j}=0$, and $y_{0j}=0$, $j=1,2,3$. Set II: $x_{0j}=0$, $x_{0,j+1}=\sqrt{-(\kappa+3\lambda)/\mu}$, $x_{0,j+2}=-\sqrt{-(\kappa+3\lambda)/\mu}$, and $y_{0j}=0$, $j=1,2,3$ mod 3. Set III: $x_{0,1}=((\kappa+\lambda)x_{0,2}+\mu x_{0,2}^3)/\lambda$, $x_{0,3}=x_{0,2}$ and $y_{0j}=0$, where $x_{0,2}$ is obtained from

$$\mu^3 x_{0,2}^6+(2\kappa\mu^2+3\mu^2\lambda)x_{0,2}^4+(\kappa^2\mu+3\kappa\mu\lambda+3\mu\lambda^2)x_{0,2}^2+(\kappa+3\lambda)\lambda^2=0,$$

The trivial equilibrium solution in set I corresponds to the zero-mean oscillations of the coupled system in which the gyroscopes are fully synchronized, i.e., they all oscillate with the same phase and same amplitude. Recall that numerical simulations indicate that this solution is unstable for $\lambda\le\lambda_c$ and stable when $\lambda>\lambda_c$. When $\lambda\le\lambda_c$, in particular, numerical simulations further show that two of the gyroscopes are always oscillating with the same mean-average while the third one exhibits a different mean average. This type of solution seems to correspond to solution set III above, which we solve analytically via Maple but the analytical expressions for x_{02} is to cumbersome to show it explicitly in here. Note also that Eq. (B2b) indicates that the mean values of the oscillations along the sensing axis undergo a subcritical pitchfork bifurcation at $\kappa=0$. Since $\kappa>0$ and $\mu>0$, the only feasible mean-value solution in all sets is $y_{0j}=0$.

Now, collecting $O(\varepsilon)$ terms we get:

$$mw_d^2\frac{\partial^2 x_{1j}}{\partial \xi^2}+cw_d\frac{\partial x_{1j}}{\partial \xi}+\kappa x_{1j}+3\mu x_{0j}^2 x_{1j}=2m\Omega_z w_d\frac{\partial y_{1j}}{\partial \xi}+\lambda(x_{1,j+1}-2x_{1j}+x_{1,j-1}), \tag{B3a}$$

$$mw_d^2\frac{\partial^2 y_{1j}}{\partial \xi^2}+cw_d\frac{\partial y_{1j}}{\partial \xi}+\kappa y_{1j}+3\mu y_{0j}^2 y_{1j}=-2m\Omega_z w_d\frac{\partial x_{1j}}{\partial \xi}, \tag{B3b}$$

$$mw_d^2\frac{\partial^2 X_{1j}}{\partial \xi^2}+cw_d\frac{\partial X_{1j}}{\partial \xi}+\kappa X_{1j}+3\mu x_{0j}^2 X_{1j}=\sin w_d t+2m\Omega_z w_d\frac{\partial Y_{1j}}{\partial \xi}+\lambda(X_{1,j+1}-2X_{1j}+X_{1,j-1}), \tag{B3c}$$

$$mw_d^2\frac{\partial^2 Y_{1j}}{\partial \xi^2}+cw_d\frac{\partial Y_{1j}}{\partial \xi}+\kappa Y_{1j}+3\mu y_{0j}^2 Y_{1j}=-2m\Omega_z w_d\frac{\partial X_{1j}}{\partial \xi}, \tag{B3d}$$

where $X_{1j}=A_{1j}\cos\xi+B_{1j}\sin\xi$ and $Y_{1j}=C_{1j}\cos\xi+D_{1j}\sin\xi$. Solving Eqs. (B3a) and (B3b) we get $x_{1j}=y_{1j}=0$, $j=1,2,3$. Solving Eqs. (B3c) and (B3d) leads to an algebraic linear system of equations for A_{1j}, B_{1j}, C_{1j}, and D_{1j}, $j=1,2$, of the form

$$\begin{bmatrix} M_{11} & M_{12} & -2\lambda I_2 & O_2 \\ -M_{12} & M_{22} & O_2 & O_2 \\ -\lambda I_2 & O_2 & M_{33} & M_{12} \\ O_2 & O_2 & -M_{12} & M_{22} \end{bmatrix} V=\vec{b_1},$$

where $V=[A_{11},B_{11},C_{11},D_{11},A_{12},B_{12},C_{12},D_{12}]^T$, $b_1=[0,1,0,0,0,1,0,0]^T$, I_2 is the identity matrix of dimensions 2×2, O_2 is the zero matrix also of dimensions 2×2,

$$M_{11}=\begin{bmatrix} m_{11} & cw_d \\ -cw_d & m_{11} \end{bmatrix},\quad M_{12}=\begin{bmatrix} 0 & -2m\Omega \\ 2m\Omega & 0 \end{bmatrix},$$

where $m_{11}=-mw_d^2+\kappa+3\mu x_{01}^2+2\lambda$. Also,

$$M_{22}=\begin{bmatrix} m_{22} & cw_d \\ -cw_d\Omega & m_{22} \end{bmatrix},\quad M_{33}=\begin{bmatrix} m_{33} & cw_d \\ -cw_d & m_{33} \end{bmatrix},$$

where $m_{22}=-mw_d^2+\kappa$ and $m_{33}=-mw_d^2+\kappa+3\mu x_{02}^2+\lambda$. We solve the resulting system of equations analytically via Maple which yields a unique solution but we do not express that solution explicitly for brevity.

Now, collecting $O(\varepsilon^2)$ terms we get

$$mw_d^2\frac{\partial^2 x_{2j}}{\partial \xi^2}+cw_d\frac{\partial x_{2j}}{\partial \xi}+\kappa x_{2j}+3\mu x_{0j}\left(x_{0j}x_{2j}+\frac{3}{2}\|X_{1j}\|^2\right)=2m\Omega_z w_d\frac{\partial y_{2j}}{\partial \xi}+\lambda(x_{2,j+1}-2x_{2j}+x_{2,j-1}), \tag{B4a}$$

$$mw_d^2\frac{\partial^2 y_{2j}}{\partial \xi^2}+cw_d\frac{\partial y_{2j}}{\partial \xi}+\kappa y_{2j}+3\mu y_{0j}^2 y_{2j}=-2m\Omega_z w_d\frac{\partial x_{2j}}{\partial \xi}, \tag{B4b}$$

$$mw_d^2\frac{\partial^2 X_{2j}}{\partial \xi^2}+cw_d\frac{\partial X_{2j}}{\partial \xi}+\kappa X_{2j}+3\mu x_{0j}\left(x_{0j}X_{2j}+\frac{3}{2}\|X_{1j}\|^2\right)=2m\Omega_z w_d\frac{\partial Y_{2j}}{\partial \xi}+\lambda(X_{2,j+1}-2X_{2j}+X_{2,j-1}), \tag{B4c}$$

$$mw_d^2\frac{\partial^2 Y_{2j}}{\partial \xi^2}+cw_d\frac{\partial Y_{2j}}{\partial \xi}+\kappa Y_{2j}+3\mu y_{0j}^2 Y_{2j}=-2m\Omega_z w_d\frac{\partial X_{2j}}{\partial \xi}, \tag{B4d}$$

where $\|X_{1j}\|^2=A_{1j}^2+B_{1j}^2$, $X_{2j}=A_{2j}\cos\xi+B_{2j}\sin\xi+E_{2j}\cos 2\xi+F_{2j}\sin 2\xi$ and $Y_{2j}=C_{2j}\cos\xi+D_{2j}\sin\xi+G_{2j}\cos 2\xi+H_{2j}\sin 2\xi$. Solving Eq. (B4a) and (B4b) we get:

$$x_{21}=-\frac{3\mu}{2\Delta}[x_{01}\delta_{21}(A_{11}^2+B_{11}^2)+2x_{02}\lambda(A_{12}^2+B_{12}^2)],$$

$$x_{22} = -\frac{3\mu}{2\Delta}[x_{01}\lambda(A_{11}^2 + B_{11}^2) + x_{02}\delta_{22}(A_{12}^2 + B_{12}^2)],$$

$$x_{32} = x_{22},$$

where $\delta_{21}=\kappa+3x_{02}^2\mu+\lambda$, $\delta_{22}=\kappa+3x_{01}^2\mu+2\lambda$, $\Delta=(\kappa+3x_{01}^2\mu+2\lambda)(\kappa+3x_{02}^2\mu+\lambda)-2\lambda^2$. Solving Eqs. (B4c) and (B4d) we get $A_{2j}=B_{2j}=C_{2j}=D_{2j}=0$ for all $j=1,2,3$. But for E_{2j}, F_{2j}, G_{2j}, and H_{2j}, $j=1,2$, we get an algebraic linear system of equations of the form

$$\begin{bmatrix} N_{11} & N_{12} & -2\lambda I_2 & O_2 \\ -N_{12} & N_{22} & O_2 & O_2 \\ -\lambda I_2 & O_2 & N_{33} & N_{12} \\ O_2 & O_2 & -N_{12} & N_{22} \end{bmatrix} W = \vec{b_2},$$

where $W=[E_{21},F_{21},G_{21},H_{21},E_{22},F_{22},G_{22},H_{22}]^T$, $\vec{b_2}=[0,1,0,1,0,0,0,0]^T$, I_2 is the identity matrix of dimensions 2×2, O_2 is the zero matrix also of dimensions 2×2,

$$N_{11} = \begin{bmatrix} n_{11} & 2cw_d \\ -2cw_d & n_{11} \end{bmatrix}, \quad N_{12} = \begin{bmatrix} 0 & -2m\Omega \\ 2m\Omega & 0 \end{bmatrix},$$

where $n_{11}=-4mw_d^2+\kappa+3\mu x_{01}^2+2\lambda$. Also,

$$N_{22} = \begin{bmatrix} n_{22} & 2cw_d \\ -2cw_d\Omega & n_{22} \end{bmatrix}, \quad N_{33} = \begin{bmatrix} n_{33} & 2cw_d \\ -2cw_d & n_{33} \end{bmatrix},$$

where $n_{22}=-4mw_d^2+\kappa$ and $n_{33}=-4mw_d^2+\kappa+3\mu x_{02}^2+\lambda$. We solve the resulting system of equations analytically via Maple which yields a unique solution but we do not express that solution explicitly for brevity.

APPENDIX C: STABILITY

Now we need to address the stability properties of the synchronized state. In particular, we seek to find conditions on the system parameters that can help us explain the nature of the subcritical pitchfork bifurcation that leads to the creation of the synchronized state, recall Fig. 4. We start by defining a dimensionless time $\tau=t/T$, where T is a characteristic time scale to be determined. Applying the chain rule, the dimensionless equations of motion, after dividing by m, become

$$\frac{1}{T^2}\ddot{x}_j + \frac{c}{mT}\dot{x}_j + w_0^2 x_j + \frac{\mu}{m}x_j^3 = \frac{A_d}{m}\sin(w_d T\tau) + \frac{2m\Omega_z}{T}\dot{y}_j + \frac{\lambda}{m}(x_{j+1} - 2x_j + x_{j-1}),$$

$$\frac{1}{T^2}\ddot{y}_j + \frac{c}{mT}\dot{y}_j + w_0^2 y_j + \frac{\mu}{m}y_j^3 = -\frac{2m\Omega_z}{T}\dot{x}_j.$$

We are interested in the regime where the first-derivative terms are $O(1)$ while the second-order derivative term is negligible compared to all the other terms. Thus we need $c/(mT)\approx O(1)$ and $1/T^2 \ll 1$. The first of these requirements sets the time scale $T=c/m$ while the second one leads to the condition $m \ll c$. This condition corresponds to that of an overdamped spring-mass oscillator; its mass being very small, compared to the damping coefficient, so that in the absence of any external forcing the spring-mass system is always attracted to its equilibrium position. We then expect to be able to reduce the motion equations (2) to a first-order system of equations, consistent with those of an overdamped oscillator. Furthermore, the asymptotic analysis of the previous section (as well as computer simulations) show that the rotation rate Ω_z has little effect on the onset of synchronization, so if we also assume that $\Omega_z \ll 1$, we get the following reduced first-order, nonautonomous, system of differential equations

$$\dot{x}_j = -ax_j - bx_j^3 + \tilde{\lambda}(x_{j+1} - 2x_j + x_{j-1}) + \tilde{A}_d \cos ws, \tag{C1}$$

where $s=[m/(cw_0)]t$, $w=w_d/w_0$, $a=mw_0/c$, $b=\mu/(cw_0)$, $\tilde{\lambda}=\lambda/(cw_0)$, and $\tilde{A}_d=A_d/(cw_0)$, $(\dot{\cdot})$ denotes now differentiation with respect to s.

Next we apply the Lyapunov-Schmidt reduction (LS) to unravel the underlying bifurcations in Eq. (2) directly from the reduced system (C1). The calculations are similar to those carried out by Berkolaiko and Grinfeld [30] in the analysis of the multiplicity of periodic solutions in a bistable equation, except that now we are dealing with a system of coupled bistable equations. We rewrite Eq. (C1) in matrix form

$$\frac{dX}{ds} = AX - bX^3 + \tilde{A}_d \cos(ws) I_3, \tag{C2}$$

where $X=[x_1,x_2,x_3]^T$, $X^3=[x_1^3,x_2^3,x_3^3]^T$, $I_3=[1,1,1]^T$, and

$$A = \begin{bmatrix} -(a+2\tilde{\lambda}) & \tilde{\lambda} & \tilde{\lambda} \\ \tilde{\lambda} & -(a+2\tilde{\lambda}) & \tilde{\lambda} \\ \tilde{\lambda} & \tilde{\lambda} & -(a+2\tilde{\lambda}) \end{bmatrix}.$$

Let $X_0=[x_0(t),x_0(t),x_0(t)]^T$ be the synchronized periodic solution of Eq. (C2). We wish to understand the bifurcations that this solution undergoes as λ varies. We define the operator Φ by

$$\Phi(X,\tilde{\lambda}) = \dot{X} - AX + bX^3 - \tilde{A}_d \cos(wt) I_3, \tag{C3}$$

so that periodic solutions of Eq. (C2) correspond to zeros of Φ. Then the purpose of the LS procedure is to construct a reduced function $g: R\times R \to R$ so that solutions of $\Phi(X,\tilde{\lambda})=0$ are locally in one-to-one correspondence with solutions of $g(x,\tilde{\lambda})=0$, which, in principle, should be easier to calculate. Golubitsky and Schaeffer [31] outline a procedure to calculate g and its derivatives though they also caution that "in realistic applications it is never possible to derive an explicit formula for $g(x,\tilde{\lambda})$." Nevertheless, in most cases it is still possible to compute the derivatives of g at the bifurcation point, which should suffice to unravel the stability properties of the periodic solution [32].

Let $L=(d\Phi)_{(X_0,\tilde{\lambda}_c)}$ be the linearization of Eq. (C3) at the critical point $(X_0,\tilde{\lambda}_c)$. In the first step of the LS reduction we need to choose orthogonal complements $M=(\mathrm{Ker}\, L)^{\perp}$ and

$N=(\text{range } L)^{\perp}$. By assumption, a bifurcation occurs at the critical point $(X_0,\tilde{\lambda}_c)$ so that $\text{Ker } L\neq\{0\}$. So we should be able to find a basis for Ker L and $(\text{Range } L)^{\perp}$. We start with Ker L, in which case direct calculations yield

$$LV=(d\Phi)_{(X_0,\tilde{\lambda}_c)}V=\dot{V}-(A-3bX_0^2)V,$$

where $X_0^2=[x_0^2,x_0^2,x_0^2]^T$. It follows that $V\in\text{Ker } L$ if and only if V is a solution of the linear system

$$\dot{V}=(A-3bX_0^2)V. \tag{C4}$$

Using the transformation $V=PW$, in which P is the matrix

$$P=\frac{1}{3}\begin{bmatrix}-1 & -1 & 1\\ -1 & 0 & 1\\ 2 & 1 & 1\end{bmatrix},$$

we can rewrite Eq. (C4) as $\dot{W}=[P^{-1}(A-3bX_0^2)P]W$, where

$$P^{-1}(A-3bX_0^2)P=\begin{bmatrix}-\sigma-3bx_0^2 & 0 & 0\\ 0 & -\sigma-3bx_0^2 & 0\\ 0 & 0 & -a-3bx_0^2\end{bmatrix},$$

is the Jordan canonical form of $(A-3bX_0^2)$ and $\sigma=(a+3\tilde{\lambda})$. Solving for W is then straightforward

$$W(t)=\exp\left(-\sigma t-3b\int_0^t x_0^2ds\right)W_1+\exp\left(-at-3b\int_0^t x_0^2ds\right)W_2,$$

where W_1 is any vector in the two-dimensional subspace $[x,y,0]^T$ while $W_2=[0,0,1]^T$. More importantly, this shows that $\text{Ker } L=\text{span}\{V_1,V_2\}$, where the basis elements are

$$V_1=\exp\left(-\sigma t-3b\int_0^t x_0^2ds\right)P^{-1}W_1P,$$

$$V_2=\exp\left(-at-3b\int_0^t x_0^2ds\right)P^{-1}W_1P.$$

We now turn to the computation of a basis for $(\text{Range } L)^{\perp}$. Since L is a self-adjoint operator then $(\text{Range } L)^{\perp}=L^*$, so that

$$L^*V=(d\Phi)_{(X_0,\tilde{\lambda}_c)}V=\dot{V}+(A-3bX_0^2)V.$$

Similar calculations lead to $\text{Ker } L^*=\text{span}\{V_1^*,V_2^*\}$, where the basis elements are

$$V_1^*=\exp\left(\sigma t+3b\int_0^t x_0^2ds\right)P^{-1}W_1P,$$

$$V_2^*=\exp\left(at+3b\int_0^t x_0^2ds\right)P^{-1}W_1P.$$

It follows from these previous calculations that $\dim(\text{Ker } L)=2$, so that $g=(g_1,g_2)$. This result was already expected on the basis of the $\mathbf{D}_3$ symmetry of the array of gyroscopes. That is, it is well known that bifurcation problems in systems with symmetry generically lead to reduced equations with multiple critical eigenvalues, mathematically this means $\dim(\text{Ker } L)\geq 2$.

Now that we have found bases for Ker L and Ker L^* we can write the bifurcation problem as

$$g_i(0,\tilde{\lambda}_c)=0 \tag{C5a}$$

$$\frac{\partial g_i}{\partial x_i}(0,\tilde{\lambda}_c)=0. \tag{C5b}$$

Equation (C5a) is simply the zeros of g which are in one-to-one correspondence with the periodic solutions of $\Phi(X,\tilde{\lambda})=0$ while Eq. (C5b) are the zero-eigenvalue conditions or the bifurcation condition of the problem. Other derivatives of g at the bifurcation point $(0,\tilde{\lambda}_c)$ are given by

$$\frac{\partial g_i}{\partial\tilde{\lambda}}=\langle V_i^*,\Phi_{\tilde{\lambda}}\rangle, \tag{C6a}$$

$$\frac{\partial^2 g_i}{\partial x_j^2}=\langle V_i^*,d^2\Phi(V_j,V_j)\rangle, \tag{C6b}$$

$$\frac{\partial^2 g_i}{\partial x_j\,\partial\tilde{\lambda}}=\langle V_i^*,(d\Phi_{\tilde{\lambda}})\cdot V_j-d^2\Phi(V_j,L^{-1}E\Phi_{\tilde{\lambda}})\rangle, \tag{C6c}$$

$$\frac{\partial^3 g_i}{\partial x_j^3}=\langle V_i^*,d^2\Phi(V_j,V_j,V_j)\rangle. \tag{C6d}$$

Direct calculations (not shown for brevity) yield the following results:

$$\frac{\partial g_i}{\partial\tilde{\lambda}}=0, \tag{C7a}$$

$$\frac{\partial^2 g_i}{\partial x_j^2}=0, \tag{C7b}$$

$$\frac{\partial^2 g_i}{\partial x_j\,\partial\tilde{\lambda}}=-\frac{w}{2\pi}\frac{\partial}{\partial\tilde{\lambda}}\int_0^{2\pi/w}\sigma_i ds, \tag{C7c}$$

$$\frac{\partial^3 g_i}{\partial x_j^3}=\frac{3bw}{\pi}\int_0^{2\pi/w}\|V_i\|^2 ds, \tag{C7d}$$

where σ_i is the ith eigenvalue of the linearization of Eq. (C2) about X_0. For the synchronization state to be stable we must have $\sigma_i<0$, for all i, which yields the stability condition

$$\frac{\partial^2 g_i}{\partial x_j \partial \tilde{\lambda}} \geq 0.$$

Finally, Eq. (C6d) is the nondegenerate condition that controls the direction of the bifurcation. Since the sign of $(g_i)_{xxx}$ is determined by b it follows that when $b>0$ the pitchfork bifurcation at which three periodic solutions of Eq. (C1) merge to form the synchronized solution is supercritical. Similarly, when $b<0$ the pitchfork bifurcation is subcritical.

[1] M. Inchiosa, A. Bulsara, K. Wiesenfeld, and L. Gammaitoni, Phys. Lett. A **252**, 20 (1999).
[2] W. Bornhofft and G. Trenkler, *Sensors, a Comprehensive Survey* (VCH, New York, 1989), Vol. 5.
[3] J. P. Wikswo, in *Applications of Superconductivity*, edited by H. Weinstock (Kluwer Academic Publishers, The Netherlands, 2000).
[4] A. R. Bulsara, C. Seberino, L. Gammaitoni, M. F. Karlsson, B. Lundqvist, and J. W. C. Robinson, Phys. Rev. E **67**, 016120 (2003).
[5] M. Inchiosa, V. In, A. Bulsara, K. Wiesenfeld, T. Heath, and M. Choi, Phys. Rev. E **63**, 066114 (2001).
[6] A. R. Bulsara, V. In, A. Kho, P. Longhini, A. Palacios, W. J. Rappel, J. Acebron, S. Baglio, and B. Ando, Phys. Rev. E **70**, 036103 (2004).
[7] V. In, A. R. Bulsara, A. Palacios, P. Longhini, A. Kho, and J. D. Neff, Phys. Rev. E **68**, 045102(R) (2003)
[8] A. R. Bulsara, V. In, A. Kho, A. Palacios, P. Longhini, J. Neff, G. Anderson, C. Obra, S. Baglio, and B. Ando, Meas. Sci. Technol. **19**, 075203 (2008).
[9] V. In, A. Kho, J. D. Neff, A. Palacios, P. Longhini, and B. K. Meadows, Phys. Rev. Lett. **91**, 244101 (2003).
[10] L. Oropeza-Ramos and K. Turner, in IEEE Sensors 2005 (IEEE, Piscataway, 2005), pp. 660–663.
[11] D. Fogliatti, in IEEE International Symposium on Circuits and Systems IV (IEEE, Piscataway, 2002), pp. 289–292.
[12] S. Baglio, A. Bulsara, J. Neff, and N. Savalli, *Array of Coupled CMOS Resonant Vibrating Gyroscopes*, in Proceedings of Eurosensors 2004 XVIII (Rome, Italy, 2004), pp. 466–467.
[13] D. Fogliatti, B. Meadows, J. Neff, V. In, and A. Bulsara, United States Patent No. 6,880,400 (19 April, 2005.
[14] Source, http://en.wikipedia.org/wiki/Coriolis_effect
[15] V. Apostolyuk, *MEMS/NEMS Handbook* (Springer, New York, 2006), Vol. 1, pp. 173–195.
[16] V. Apostolyuk and F. Tay, Sens. Lett. **2**, 252 (2004).
[17] A. Shkel, IEEE/ION PLANS 2006, 586–593. San Diego, CA, USA.
[18] A. Nayfeh, *Perturbation Methods* (Wiley-VCH, New York, 2004).
[19] R. Rand, Lectures Notes on Nonlinear Vibrations.
[20] B. Van der Pol, London, Edinburgh Dublin Philos. Mag. J. Sci. Series 7 Vol. **2**, 978 (1926).
[21] N. Krylov and N. Bogoliubov, Introduction to Nonlinear Mechanics (in Russian). Kiev, 1937, Izd. AN UkSSR, Vvedenie v Nelineinikhu Mekhaniku.
[22] E. V. Appleton, Proc. Cambridge Philos. Soc. **21**, 231 (1922).
[23] B. van der Pol, Philos. Mag. **3**, 64 (1927).
[24] B. van der Pol, Nature (London) **120**, 363 (1927).
[25] P. Holmes and D. R. Rand, Q. Appl. Math. **35**, 495 (1978).
[26] J. Argyris, G. Faust, and M. Haase, *An Exploration of Chaos* (North-Holland, Amsterdam, 1994).
[27] S. Wiggins, *Introduction to Applied Nonlinear Dynamical Systems* (Springer-Verlag, New York, 1990).
[28] P. Ashwin and J. W. Swift, J. Nonlinear Sci. **2**, 69 (1992).
[29] E. Doedel and X. Wang. Auto94: *Software for Continuation and Bifurcation Problems in Ordinary Differential Equations*, Applied Mathematics Report, California Institute of Technology, July 1994.
[30] G. Berkolaiko and M. Grinfeld, Proc. R. Soc. A **462**, 1001 (2006).
[31] M. Golubitsky, I. N. Stewart, and D. G. Schaeffer, *Singularities and Groups in Bifurcation Theory: Vol. I*, Appl. Math. Sci. Vol. 69, (Springer-Verlag, New York, 1988).
[32] D. Cox and H. Miller, *Stochastic Processes* (Chapman and Hall, London, 1996).